European Journal of Mechanics A/Solids 34 (2012) 120–129

Contents lists available at SciVerse ScienceDirect

European Journal of Mechanics A/Solids

journal homepage: www.elsevier.com/locate/ejmsol

In-plane elastic buckling of hierarchical honeycomb materials

Qiang Chen [a], Nicola M. Pugno [a,b,c,*]

[a] Laboratory of Bio-Inspired Nanomechanics "Giuseppe Maria Pugno", Department of Structural Engineering and Geotechnics, Politecnico di Torino, 10129, Torino, Italy
[b] National Institute of Nuclear Physics, National Laboratories of Frascati, Via E. Fermi 40, 00044, Frascati, Italy
[c] National Institute of Metrological Research, Strada delle Cacce 91, I-10135, Torino, Italy

ARTICLE INFO

Article history:
Received 29 July 2011
Accepted 23 December 2011
Available online 12 January 2012

Keywords:
Hierarchical honeycomb
Local buckling stress
Progressive failure
Energy absorption

ABSTRACT

In this paper, we study the elastic buckling of a new class of honeycomb materials with hierarchical architecture, which is often observed in nature. Employing the top–down approach, the virtual buckling stresses and corresponding strains for each cell wall at level $n-1$ are calculated from those at level n; then, comparing these virtual buckling stresses of all cell walls, the real local buckling stress is deduced; also, the progressive failure of the hierarchical structure is studied. Finally, parametric analyses reveal influences of some key parameters on the local buckling stress and strength-to-density ratio; meanwhile the constitutive behaviors and energy-absorption properties, with increasing hierarchy n, are calculated. The results show the possibility to tailor the elastic buckling properties at each hierarchical level, and could thus have interesting applications, e.g., in the design of multiscale energy-absorption honeycomb light materials.

1. Introduction

Honeycomb materials are widely observed in nature materials, such as the turtle shell (Krauss et al., 2009) or the lobster's exoskeleton (Fabritius et al., 2009), and they are very promising for material design (Gibson et al., 1982; Warren and Kraynik, 1987; Papka and Kyriakides, 1994, 1998a; Gibson and Ashby, 1997) due to their specific structural properties. For example, in the field of material science, they are used to be core materials in sandwich structures (Foo et al., 2007) and employed as energy-absorption materials to reduce loading impact and protect an object from crushing (Xue and Hutchinson, 2006).

Many pioneering works focused on its in-plane and out-of-plane mechanical behaviors (e.g., elastic buckling) (Papka and Kyriakides, 1998b; Zhang and Ashby, 1992); for example, Papka and Kyriakides (1994) explained the crushing process under uniaxial compression in detail. Generally, the collapse behavior of the honeycomb material is characterized by three regimes: (1) at the initial loading stage, the material has a relatively high stiffness, the deformation is caused by the bending of cell walls and it is linear-elastic and stable; (2) as load increases, the material collapses locally in a progressive but metastable way; (3) finally, the whole structure collapses during densification, the stiffness increases and the deformation is uniform and very stable. The three stages are shown in Fig. 1, in which our observations on a natural honeycomb and Scanning Electron Microscopic (SEM) images of the cell-wall constituent materials are reported.

It is well-known that Nature creates composite structures in a hierarchical way, from nanoscale to macroscale (Launey and Ritchie, 2009); the structures/materials at nanoscale and microscale exhibit highly anisotropy (Ritchie et al., 2009; Yao et al., 2011); e.g., in bioshells, they exhibit structural gradient (a so-called functional graded material), for instance, the exoskeleton of lobsters has three different layers from exterior to interior, with decreasing densities, strength and hardness (Raabe et al., 2005). Honeycomb structure enables these biological materials to exhibit outstanding mechanical properties, e.g. low weight, high stiffness, strength, and toughness (Smith et al., 1999; Munch et al., 2008). For this reason, bio-inspired materials are becoming of great interest in material science. Munch et al. (2008) recently synthesized a tough bio-inspired hybrid material based on aluminum oxide and polymethyl methacrylate, and the toughness of the product was more than 300 times higher than those of the constituent materials. The synthesized structure was lamellar and similar to that of nacre, which has two hierarchical levels. Theoretically, basing on the principle of flow tolerance, Gao (2006) brought a tensile-shear chain model forward to investigate the hierarchical mechanical properties of bone and bone-like materials; Zhang et al. (2011) reported that the hierarchy of load-bearing biological materials -was dominated by a toughness optimization.

* Corresponding author. National Institute of Metrological Research, Strada delle Cacce 91, I-10135, Torino, Italy.
E-mail address: nicola.pugno@polito.it (N.M. Pugno).

0997-7538/$ – see front matter © 2011 Elsevier Masson SAS. All rights reserved.
doi:10.1016/j.euromechsol.2011.12.003

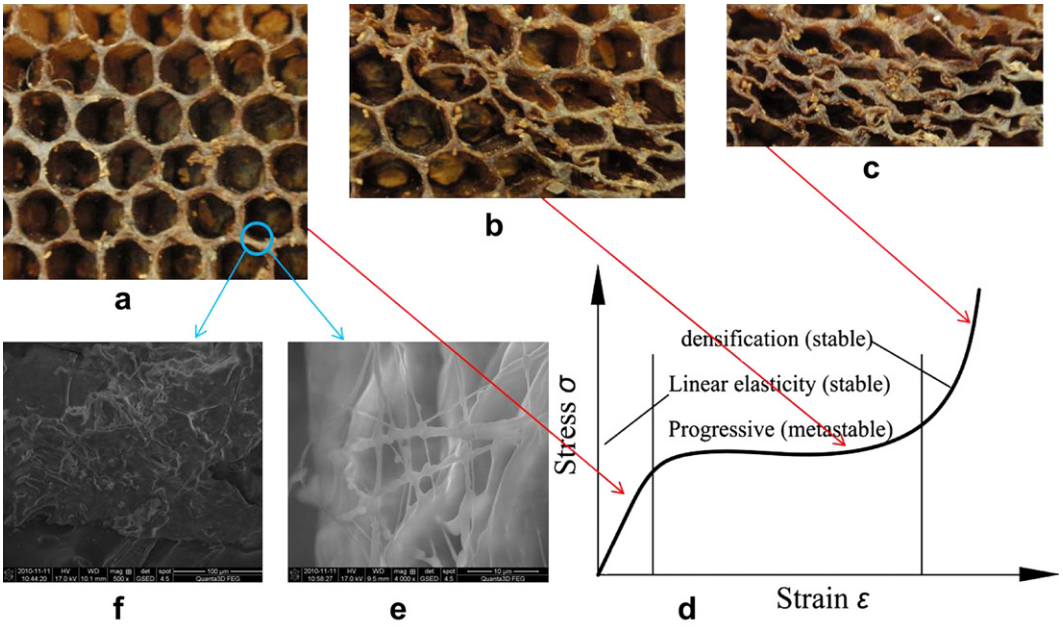

Fig. 1. Natural honeycomb crushing process: (a) linear-elastic stable stage; (b) progressive metastable stage; (c) densification very stable stage; (d) schematic of a honeycomb stress–strain curve; (e) silk (inclusion); (f) wax grain (matrix).

As for the studies on hierarchical honeycombs, Côté et al. (2009) studied the out-of-plane compressive properties of a composite square honeycomb sandwich core with structural hierarchy, and reported that the hierarchical topology substantially increased its compressive strength. Taylor et al. (2011) introduced hierarchy into honeycomb structures with different geometries (i.e., hexagonal, triangular or squared), and investigated the in-plane elastic properties of honeycombs influenced by structural hierarchy; the results showed that hierarchy generally deterred the mechanical behavior of the hierarchical honeycomb, but interestingly, the negative Poisson's ratio substructure resulted in a higher density modulus. Besides, Sen et al. (2011) studied the size-dependent mechanical properties of a nano-sized honeycomb silica structure, and the authors found that nano-sized honeycomb silica structure was tougher than that at larger size.

In this paper, inspired by the hierarchical structure of natural materials (Fig. 2) (Cai, 2007; Gibson, 2005) and starting from an orthotropic material, we construct a new hierarchical honeycomb material (Pugno, 2006; Pugno et al., 2008; Chen and Pugno, 2011, 2012; Pugno and Carpinteri, 2008), see Fig. 3. Extending the Euler critical load of isotropic to orthotropic columns by pure bending beam theory, the local buckling stress of the hierarchical honeycomb material is formulated due to the significance in the energy-absorption mechanism. Besides, we perform a parametric analysis to investigate the influences of relevant parameters on local buckling loads, strength-to-density ratio, virtual progressive failure, constitutive law and energy-absorption behavior.

2. Elastic buckling of hierarchical honeycomb

Here, cell walls are treated as columns, as done in the classical theory of non-hierarchical honeycomb (Gibson and Ashby, 1997). For an orthotropic column, assuming the conservation of the plane sections and neglecting the shear effect, the buckling load P_{cr} becomes (Timoshenko and Gere, 1961; Tolf, 1985):

$$P_{cr} = \frac{\lambda^2 \pi^2 E_1 I}{l^2} \tag{1}$$

where, l is the length of the column, λ is a numerical factor depending on boundary conditions, E_1 is the Young's modulus in the longitudinal direction of the column and $E_1 I$ is the bending rigidity. Eq. (1) is the classical Euler buckling formula, in which the Young's modulus of an isotropic material is substituted by the longitudinal one of the orthotropic column.

2.1. Elastic buckling of the n^{th} hierarchical column

We treat the structure reported in Fig. 4a as the n^{th} level structure and each cell wall as the $(n-1)^{\text{th}}$ level; the structure at each level is considered as orthotropic due to the symmetric configuration. In order to determine its buckling load at level n, we need to calculate the applied loads acting on the six cell walls; then, employing Eq. (1), we can find the buckling loads for each column. Actually, three pairs are of our interest, i.e., ①, ②, ③ (Fig. 4); moreover, only two of them (pair ①, ②) are treated because of the symmetry. For the sake of the simplicity, the cell walls ① are treated as inclined columns with one end clamped and the other fixed, and the buckling loads of the pairs ①, ② are expressed as (Chang, 2005; Gibson et al., 1982):

$$\begin{aligned} P_1^{(n)} &= \frac{P}{2\sin\theta^{(n)}} \\ P_2^{(n)} &= P \end{aligned} \tag{2}$$

with

$$P = 2sb^{(n)}l^{(n)}\cos\theta^{(n)} \tag{3}$$

where, s is the external stress; $b^{(n)}$, $l^{(n)}$ and $\theta^{(n)}$ are, respectively, the depth of the structure, the length of column ① and the angle made by column ① and the horizontal line at level n.

2.1.1. Buckling stress analysis

According to Eqs. (2) and (3), the axial loads acting on the two columns are expressed as $\overrightarrow{P^{(n)}} = (P_1^{(n)}, P_2^{(n)})^T$ with:

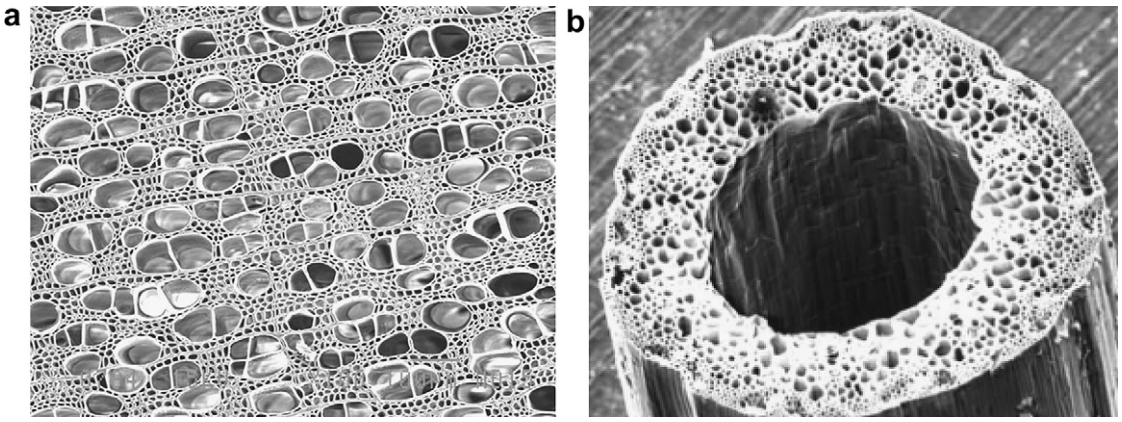

Fig. 2. SEM image of pure aspen wood: (a) aspen wood (Cai, 2007); (b) grassy stem (Gibson, 2005).

$$\begin{aligned} P_1^{(n)} &= sb^{(n)}l^{(n)}\cot\theta^{(n)} \\ P_2^{(n)} &= 2sb^{(n)}l^{(n)}\cos\theta^{(n)} \end{aligned} \tag{4}$$

Elastic collapse occurs when one of the components in the force vector $\overrightarrow{P^{(n)}}$ reaches the corresponding one in the critical force vector $\overrightarrow{P_{cr}^{(n)}} = (P_{cr,1}^{(n)}, P_{cr,2}^{(n)})^T$, namely:

$$\overrightarrow{P^{(n)}} = \overrightarrow{P_{cr}^{(n)}} \tag{5}$$

Combining Eqs. (1), (4) and (5), we find the external critical stress vector $\overrightarrow{s_{cr}^{(n)}} = (s_{cr,1}^{(n)}, s_{cr,2}^{(n)})^T$:

$$\begin{aligned} s_{cr,1}^{(n)} &= \frac{\pi^2\left(\lambda_1^{(n)}\right)^2 E_1^{(n-1)}}{12}\left(\frac{t^{(n)}}{l^{(n)}}\right)^3\tan\theta^{(n)} \\ s_{cr,2}^{(n)} &= \frac{\pi^2\left(\lambda_2^{(n)}\right)^2 E_1^{(n-1)}}{24}\left(\frac{t^{(n)}}{h^{(n)}}\right)^2\left(\frac{t^{(n)}}{l^{(n)}}\right)\sec\theta^{(n)} \end{aligned} \tag{6}$$

where, $h^{(n)}$ is the length of column ②.

Regarding the numerical factors, $\lambda_1^{(n)}$ and $\lambda_2^{(n)}$, they are determined in different ways. For the inclined cell walls, $\lambda_1^{(n)}$ is calculated by $((\lambda_1^{(n)}\pi)^2/(R^{(n)})^2)\cot^2\theta^{(n)} + 2(1-\cos(\lambda_1^{(n)}\pi)/(\lambda_1^{(n)}\pi)\sin(\lambda_1^{(n)}\pi)) - 1 = 0$ (Chang, 2005), where, $R^{(n)}$ is the slenderness ratio; here, $\lambda_1^{(n)}$ is considered as a constant and equals to 2.76, because it has a minor variation for $\theta^{(n)}$ between 15° and 75° and $R^{(n)}$ between 50 and 500; moreover, $\lambda_1^{(n)} = 2.76$, for $\theta^{(n)} = 15°$, is conservative, compared with the value of 2.86, for $\theta^{(n)} = 75°$. For the vertical cell wall we use the formula (Gibson and Ashby, 1997) $\lambda_2^{(n)}\tan\lambda_2^{(n)} = 2h^{(n)}/l^{(n)}$ to calculate $\lambda_2^{(n)}$, which depends on $h^{(n)}/l^{(n)}$. The second expression in Eq. (6) is the same as that reported by Gibson and Ashby (1997) for non-hierarchical honeycomb. The Young's modulus ($E_1^{(n-1)}$) of the cell walls is expressed as (Gibson and Ashby, 1997; Chen and Pugno, 2012):

$$E_1^{(n-1)} = \prod_{i=1}^{n-1}\left(\xi^{(i)}\left(\frac{t^{(i)}}{l^{(i)}}\right)^3\right)\cdot E_1^{(0)} \tag{7}$$

with

$$\xi^{(i)} = \frac{\left(h^{(i)}/l^{(i)} + \sin\theta^{(i)}\right)}{\cos^3\theta^{(i)}} \tag{8}$$

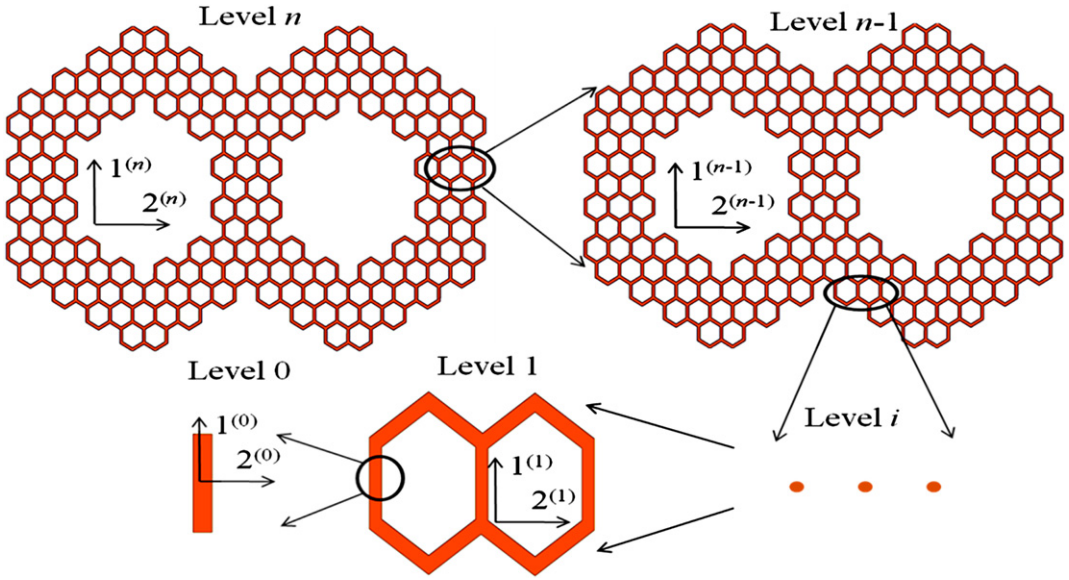

Fig. 3. Hierarchical honeycombs.

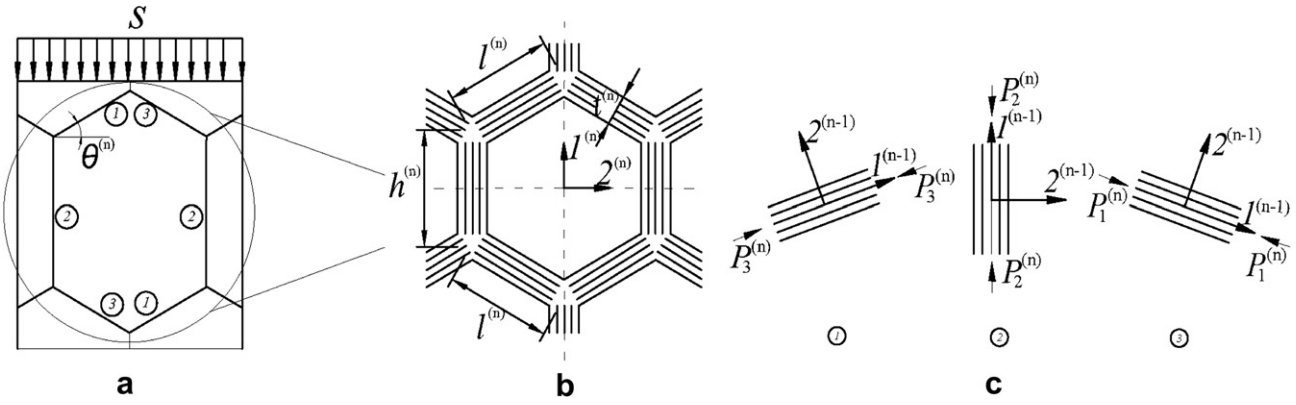

Fig. 4. Schematic of n^{th} level hierarchical honeycombs.

If we define a new pseudo-vector $\overrightarrow{\omega^{(n)}} = (\omega_1^{(n)}, \omega_2^{(n)})^T$:

$$\begin{aligned} \omega_1^{(n)} &= \cot\theta^{(n)} \\ \omega_2^{(n)} &= 2\cos\theta^{(n)} \end{aligned} \tag{9}$$

then, Eq. (4) can be rewritten as:

$$\overrightarrow{P^{(n)}} = \left(sA^{(n)}\frac{l^{(n)}}{t^{(n)}}\right) \otimes \overrightarrow{\omega^{(n)}} \tag{10}$$

where $\otimes$ is the Kronecker product and $A^{(n)} = b^{(n)}t^{(n)}$ is the cross-sectional area of the cell wall at the n^{th} level.

Correspondingly, Eq. (6) is expressed as:

$$\begin{aligned} s_{cr,1}^{(n)} &= \frac{\pi^2\left(\lambda_1^{(n)}\right)^2 E_1^{(n-1)}}{12}\left(\frac{t^{(n)}}{l^{(n)}}\right)^3 \frac{1}{\omega_1^{(n)}} \\ s_{cr,2}^{(n)} &= \frac{\pi^2\left(\lambda_2^{(n)}\right)^2 E_1^{(n-1)}}{12}\left(\frac{t^{(n)}}{h^{(n)}}\right)^2 \left(\frac{t^{(n)}}{l^{(n)}}\right) \frac{1}{\omega_2^{(n)}} \end{aligned} \tag{11}$$

Furthermore, Eq. (11) is expressed as:

$$\overrightarrow{s_{cr}^{(n)}} = \left[K_s^{(n)}\right]\left(\overrightarrow{\omega^{(n)}}\right)^{-1} E_1^{(n-1)} \tag{12}$$

where,

$$\left[K_s^{(n)}\right] = \frac{\pi^2}{12}\mathrm{diag}\left(\left(\lambda_1^{(n)}\right)^2\left(\frac{t^{(n)}}{l^{(n)}}\right)^3, \quad \left(\lambda_2^{(n)}\right)^2\left(\frac{t^{(n)}}{h^{(n)}}\right)^2\left(\frac{t^{(n)}}{l^{(n)}}\right)\right)$$

$$\left(\overrightarrow{\omega^{(n)}}\right)^{-1} = \left(\frac{1}{\omega_1^{(n)}}, \frac{1}{\omega_2^{(n)}}\right)^T$$

Accordingly, the local buckling stress at level n is the minimum one in the critical stress vector $\overrightarrow{s_{cr}^{(n)}}$, i.e.,

$$s_{cr}^{(n)} = \min\left(\overrightarrow{s_{cr}^{(n)}}\right) \tag{13}$$

2.1.2. Buckling strain analysis

In Section 2.1.1, we deduced the elastic buckling stress; whereas, in this part, the corresponding buckling strain is derived. First, we make an assumption: when one of the columns buckles, it collapses immediately and completely (see Fig. 5). Then, the displacements $\overrightarrow{\Delta\delta_{cr}^{(n)}} = (\Delta\delta_{cr,1}^{(n)}, \Delta\delta_{cr,2}^{(n)})^T$ of pair ①, ② at level n are obtained through geometrical analysis in a unit cell:

$$\begin{aligned} \Delta\delta_{cr,1}^{(n)} &= l^{(n)}\sin\theta^{(n)} \\ \Delta\delta_{cr,2}^{(n)} &= h^{(n)} \end{aligned} \tag{14}$$

and the buckling strains of pair ①, ② are $\overrightarrow{\Delta\varepsilon_{cr}^{(n)}} = (\Delta\varepsilon_{cr,1}^{(n)}, \Delta\varepsilon_{cr,2}^{(n)})^T$:

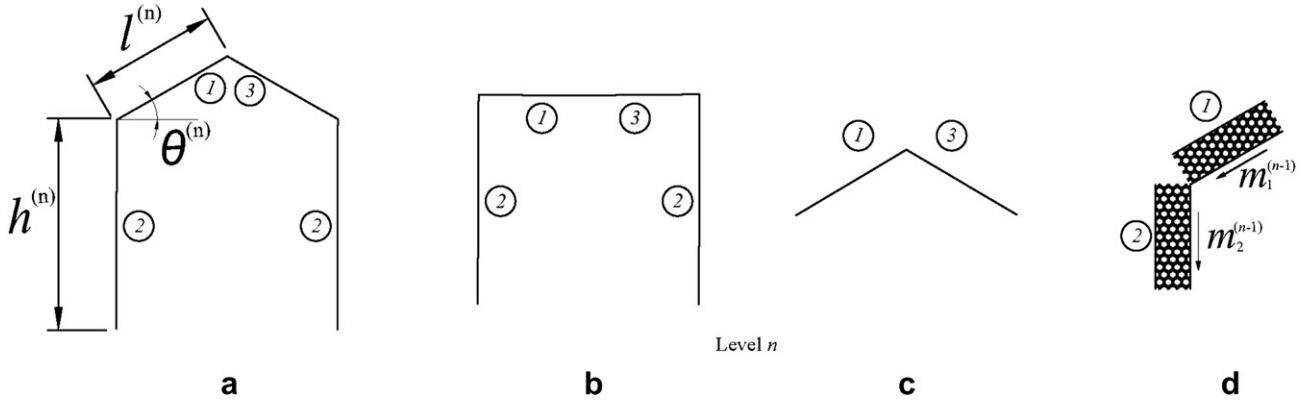

Fig. 5. Buckling collapse of n^{th} hierarchical honeycomb: (a) initial configuration; (b) collapse of columns ①, ③; (c) collapse of column ②; (d) numbers of unit cells in columns ①, ②.

$$\begin{aligned}\Delta\varepsilon_{cr,1}^{(n)} &= \frac{\Delta\delta_{cr,1}^{(n)}}{l^{(n)}\sin\theta^{(n)}+h^{(n)}}\\ \Delta\varepsilon_{cr,2}^{(n)} &= \frac{\Delta\delta_{cr,2}^{(n)}}{l^{(n)}\sin\theta^{(n)}+h^{(n)}}\end{aligned} \tag{15}$$

Thus, in general:

$$\overrightarrow{\Delta\,\varepsilon_{cr}^{(n)}} = \frac{1}{l^{(n)}\sin\theta^{(n)}+h^{(n)}}\overrightarrow{\Delta\,\delta_{cr}^{(n)}} \tag{16}$$

2.2. Elastic buckling of the $(n-1)^{th}$ level structure

2.2.1. Buckling stress analysis

Here, the $(n-1)^{\text{th}}$ level structure corresponds to the cell walls of the n^{th} level structure treated before, that is to say, each pair cell walls of the n^{th} level contains two pairs cell walls of the $(n-1)^{\text{th}}$ level structure. Thus, for the $(n-1)^{\text{th}}$ level structure, we have four pairs. Now we use the results of the n^{th} level and find the loads on the four pairs:

$$\overrightarrow{P^{(n-1)}} = \left(sA^{(n-1)}\frac{l^{(n-1)}}{t^{(n-1)}}\right)\otimes\overrightarrow{\omega^{(n)}}\otimes\overrightarrow{\omega^{(n-1)}} \tag{17}$$

Following the previous procedure, we find the critical stresses for the four pairs of cell wall at level $(n-1)$:

$$\overrightarrow{s_{cr}^{(n-1)}} = \left(\overrightarrow{\omega^{(n)}}\right)^{-1}\otimes\left(\left[K^{(n-1)}\right]\left(\overrightarrow{\omega^{(n-1)}}\right)^{-1}\right)E_1^{(n-2)} \tag{18}$$

Thus, the local buckling stress at level $(n-1)$ is derived as:

$$s_{cr}^{(n-1)} = \min\left(\overrightarrow{s_{cr}^{(n-1)}}\right) \tag{19}$$

2.2.2. Buckling strain analysis

Like level n, the displacements $\overrightarrow{\Delta\,\delta_{cr}^{(n-1)}}$ of pair ①, ② at level $(n-1)$ can be calculated as:

$$\begin{aligned}\Delta\delta_{cr,1}^{(n-1)} &= l^{(n-1)}\sin\theta^{(n-1)}\\ \Delta\delta_{cr,2}^{(n-1)} &= h^{(n-1)}\end{aligned} \tag{20}$$

If we define:

$$\overrightarrow{m^{(n-1)}} = \left(m_1^{(n)}\sin\theta^{(n)}, m_2^{(n)}\right)^T \tag{21}$$

where, $m_1^{(n)}, m_2^{(n)}$ are numbers of unit cells at level $(n-1)$ along the longitudinal direction of the columns ①, ② at level n (see Fig. 5d), the buckling strain at level $(n-1)$ is expressed as:

$$\overrightarrow{\Delta\,\varepsilon_{cr}^{(n-1)}} = \frac{1}{l^{(n)}\sin\theta^{(n)}+h^{(n)}}\overrightarrow{m^{(n)}}\otimes\overrightarrow{\Delta\,\delta_{cr}^{(n-1)}} \tag{22}$$

2.3. Elastic buckling of the first level structure

2.3.1. Buckling stress analysis

Similarly, the above stress result can be used for the first level structure by extending Eqs. (17)–(19), i.e.:

$$\overrightarrow{P^{(1)}} = \left(sA^{(1)}\frac{l^{(1)}}{t^{(1)}}\right)\otimes\overrightarrow{\omega^{(n)}}\otimes\overrightarrow{\omega^{(n-1)}}\ldots\otimes\overrightarrow{\omega^{(1)}} \tag{23}$$

The critical stresses of each pair at level 1 are:

$$\overrightarrow{s_{cr}^{(1)}} = \left(\overrightarrow{\omega^{(n)}}\right)^{-1}\otimes\left(\overrightarrow{\omega^{(n-1)}}\right)^{-1}\ldots\otimes\left(\overrightarrow{\omega^{(2)}}\right)^{-1}\otimes\left(\left[K^{(1)}\right]\left(\overrightarrow{\omega^{(1)}}\right)^{-1}\right)E_1^{(0)} \tag{24}$$

The local buckling stress at level 1 is:

$$s_{cr}^{(1)} = \min\left(\overrightarrow{s_{cr}^{(1)}}\right) \tag{25}$$

2.3.2. Buckling strain analysis

Extending Eq. (22), the buckling strain at level 1 is expressed as:

$$\overrightarrow{\Delta\,\varepsilon_{cr}^{(1)}} = \frac{1}{l^{(n)}\sin\theta^{(n)}+h^{(n)}}\overrightarrow{m^{(n)}}\otimes\overrightarrow{m^{(n-1)}}\otimes\ldots\otimes\overrightarrow{m^{(2)}}\otimes\overrightarrow{\Delta\,\delta_{cr}^{(1)}} \tag{26}$$

2.4. Local buckling stress of the whole hierarchical structure

Now, we have the local buckling loads at each level, but we usually need the buckling load for the whole structure, that is:

$$S_{cr}^{(n)} = \min\left(s_{cr}^{(1)}, s_{cr}^{(2)}, \ldots, s_{cr}^{(n)}\right) \tag{27}$$

2.5. The strength-to-density ratio

The strength-to-density ratio is an important index to design and optimize energy-absorption materials. Budiansky (1999) studied the structural efficiency of several compression structures (e.g., hollow columns and foam-filled sandwich columns) by the maximum stress and strain theory. Here, in order to evaluate the strength efficiency of the hierarchical honeycombs, we employ a strong tie provided by Ashby (2010). For a uni-axially loaded structure, the strong tie is expressed as $P_{s1} = S/\rho$, and a light but strong structure can be obtained by maximizing this value. Employing the expression of the relative density for non-hierarchical honeycombs (Gibson and Ashby, 1997), we have:

$$\frac{\rho^{(n)}}{\rho^{(n-1)}} = \frac{\left(h^{(n)}/l^{(n)}+2\right)}{2\cos\theta^{(n)}\left(h^{(n)}/l^{(n)}+\sin\theta^{(n)}\right)}\frac{t^{(n)}}{l^{(n)}} \tag{28}$$

Thus, the density of the n-level hierarchical structure is derived by an iterative process as:

$$\frac{\rho^{(n)}}{\rho^{(0)}} = \prod_{i=1}^{n}\left(\gamma^{(i)}\frac{t^{(i)}}{l^{(i)}}\right) \tag{29}$$

with

$$\gamma^{(i)} = \frac{\left(h^{(i)}/l^{(i)}+2\right)}{2\cos\theta^{(i)}\left(h^{(i)}/l^{(i)}+\sin\theta^{(i)}\right)}$$

Therefore, combining Eqs. (27) and (29), the strength-to-density is expressed as:

$$\frac{S_{cr}^{(n)}}{\rho^{(n)}} = \frac{\min\left(s_{cr}^{(1)}, s_{cr}^{(2)}, \ldots, s_{cr}^{(n)}\right)}{\rho^{(0)}\times\prod_{i=1}^{n}\left(\gamma^{(i)}\frac{t^{(i)}}{l^{(i)}}\right)} \tag{30}$$

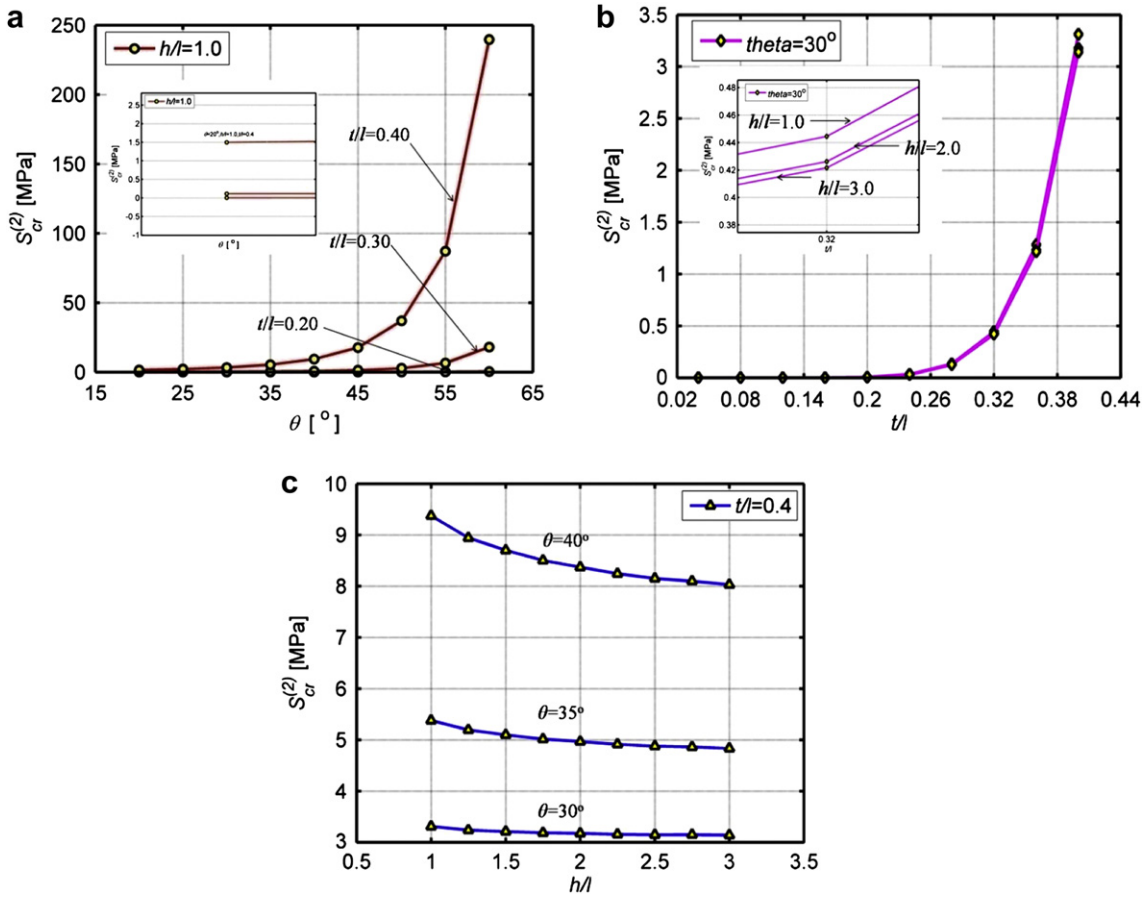

Fig. 6. Parametric analysis on the buckling stress $S_{cr}^{(2)}$ of a two-level hierarchical honeycomb. Insets in Fig. 6a, b are local magnifications, respectively.

3. Parametric analysis

The influences of the parameters in the vector $\overrightarrow{\chi^{(i)}} = (\theta^{(i)}, h^{(i)}/l^{(i)}, t^{(i)}/l^{(i)})$ are investigated under the self-similar conditions: $h^{(i)}/l^{(i)} = h/l$, $t^{(i)}/l^{(i)} = t/l$, and thus $t^{(i)}/h^{(i)} = t/h$; the boundary coefficient $\lambda_2^{(i)}$ is a function of $h^{(i)}/l^{(i)}$, as well as $\lambda_2^{(i)} = \lambda_2$. Thus, the self-similar conditions are:

$$\overrightarrow{\chi^{(i)}} = \vec{\chi} = (\theta, h/l, t/l) \quad i = 1, 2, \ldots, n \tag{31}$$

In this section, inspired by wood, we treat the example of hierarchical honeycombs. The elastic modulus $E_1^{(0)} = 10,600$ MPa and density $\rho^{(0)} = 1.5$ g/cm^3 (Easterling et al., 1982) of wood cell walls are adopted here.

3.1. Local buckling stress

Here, the local buckling stress refers to the value under which the first column takes place, see Eq. (27). Taking a two-level self-similar honeycomb, as an example, the parametric analysis results are plotted in Fig. 6.

Fig. 6 shows the influences of two components in the vector $\vec{\chi}$ with the left one fixed. We can see that the buckling stress generally increases when t/l and θ increase (Fig. 6a,c); while it decreases when h/l increases (see the inset in Fig. 6b), wheras increasing h/l produces a weak influence (Fig. 6c), compared with the previous ones. Regarding the influence on the mechanical behavior of the three geometric parameters appearing in the vector $\vec{\chi}$, we note that: increasing t/l produces a larger bending

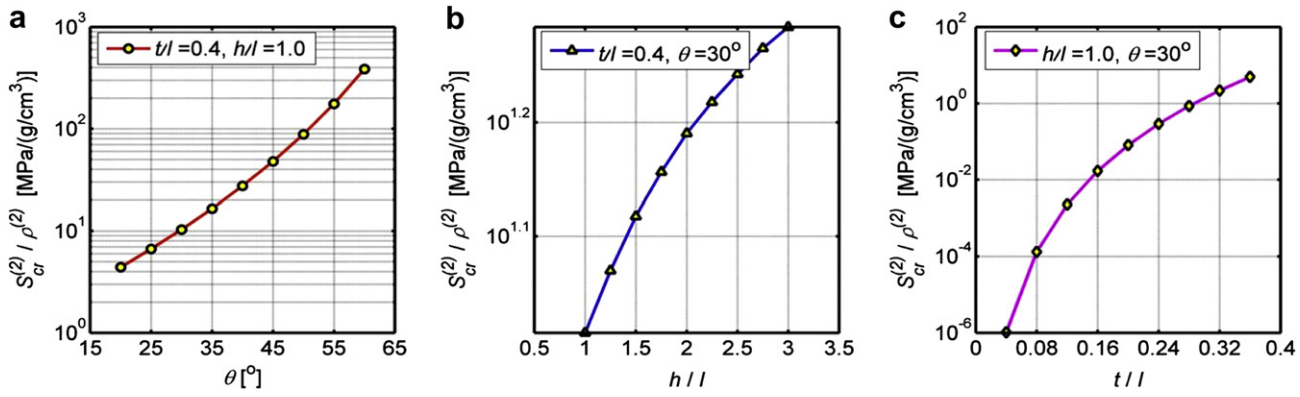

Fig. 7. Parametric analysis on the strength-to-density ratio of the two-level hierarchical honeycomb.

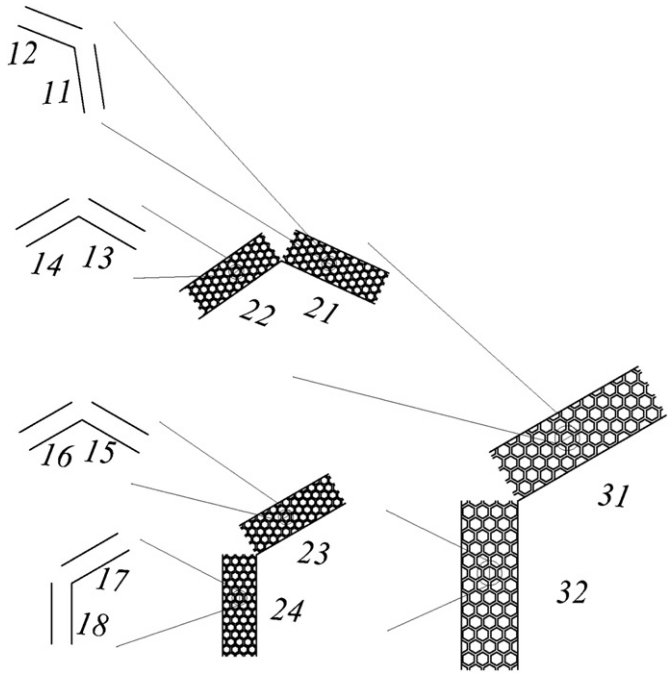

Fig. 8. Schematic of a three-level hierarchical honeycomb. The subscripts of each column reflect the location in the hierarchical structure; the first subscript denotes the level and the second its location in the level.

rigidity of the inclined columns, thus, the Young's modulus and the buckling strength are enhanced; likewise, increasing θ, with the other parameters fixed, results in larger Young's modulus (Eqs. (7) and (8)) and again in larger strengths; in contrast, the variation of h/l yields to an opposite trend. Also, we compare our result with the transverse strength of natural wood, which is defined as the stress at the proportional limit, corresponding to the first buckling stress in our model. For example, radial compression strength of *Balsa* is about 1500 kPa (Easterling et al., 1982), which results in a value of 1497 kPa at $\overrightarrow{\chi} = (20^\circ, 1.0, 0.4)$ (see the inset in Fig. 6a). Besides, more strength measurements of some important commercial woods are available in Green et al. (1999), and their transverse compression strengths range from 1000 kPa to 19000 kPa, which match our result very well by selecting the material properties.

3.2. Strength to density ratio

Based on the density value of wood, the strength-to-density ratios $S_{cr}^{(2)}/\rho^{(2)}$ of the two-level hierarchical structures influenced by θ, h/l and t/l are shown in Fig. 7.

It suggests that the strength-to-density ratio increases when one of these geometrical parameters increases. And the increase in θ or t/l is more efficient than that in h/l. The former improve the buckling-resisting capacity by approximately two or six orders of magnitude (θ from 20° to 60° and t/l from 0.04 to 0.36), while the latter is in the same order when h/l varies from 1.0 to 3.0. However, differently from Fig. 6b, Fig. 7b shows that increasing h/l results in

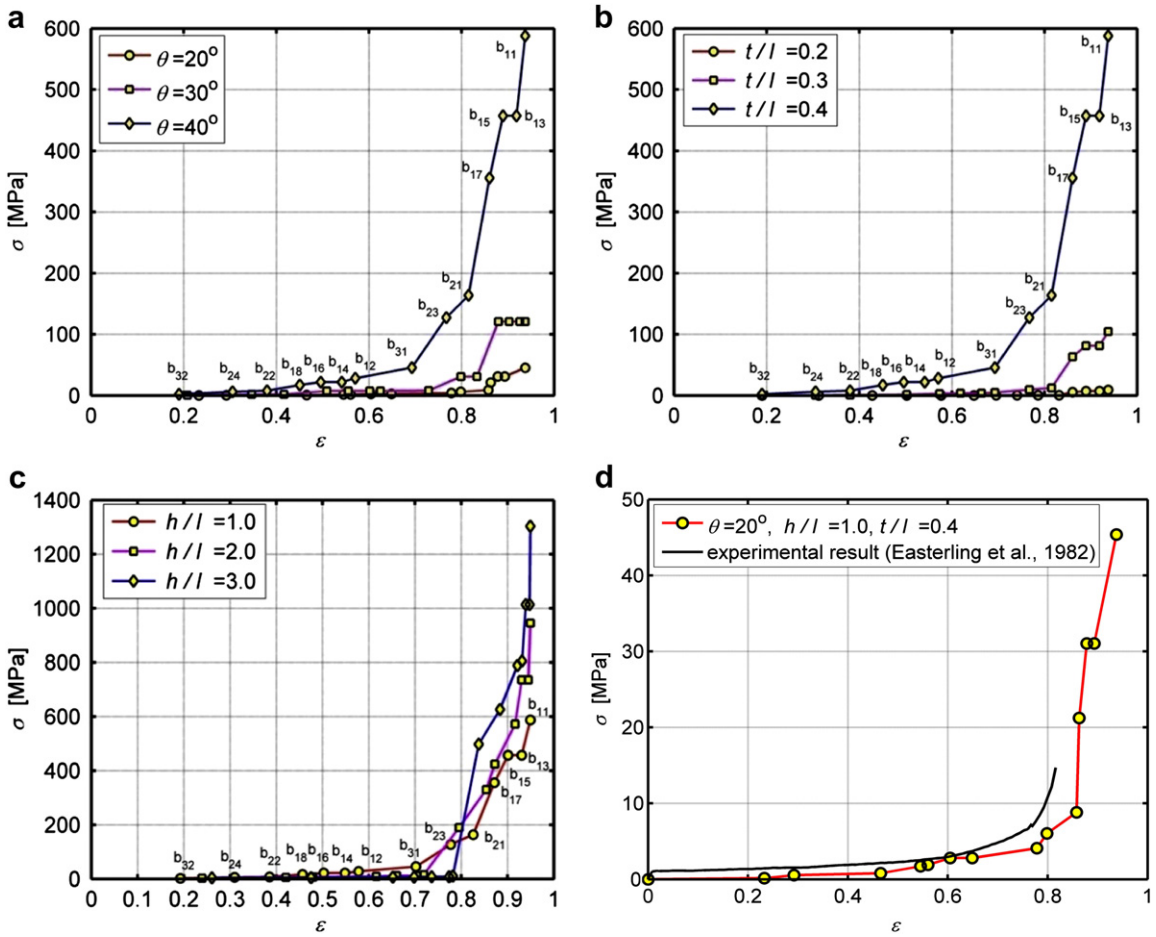

Fig. 9. Progressive failure stress–strain relationship of a three-level hierarchical honeycomb: (a) $h/l = 1.0$, $t/l = 0.1$; (b) $\theta = 40^\circ$, $t/l = 0.1$; (c) $\theta = 40^\circ$, $h/l = 1.0$; (d) comparison between theory and experiment.

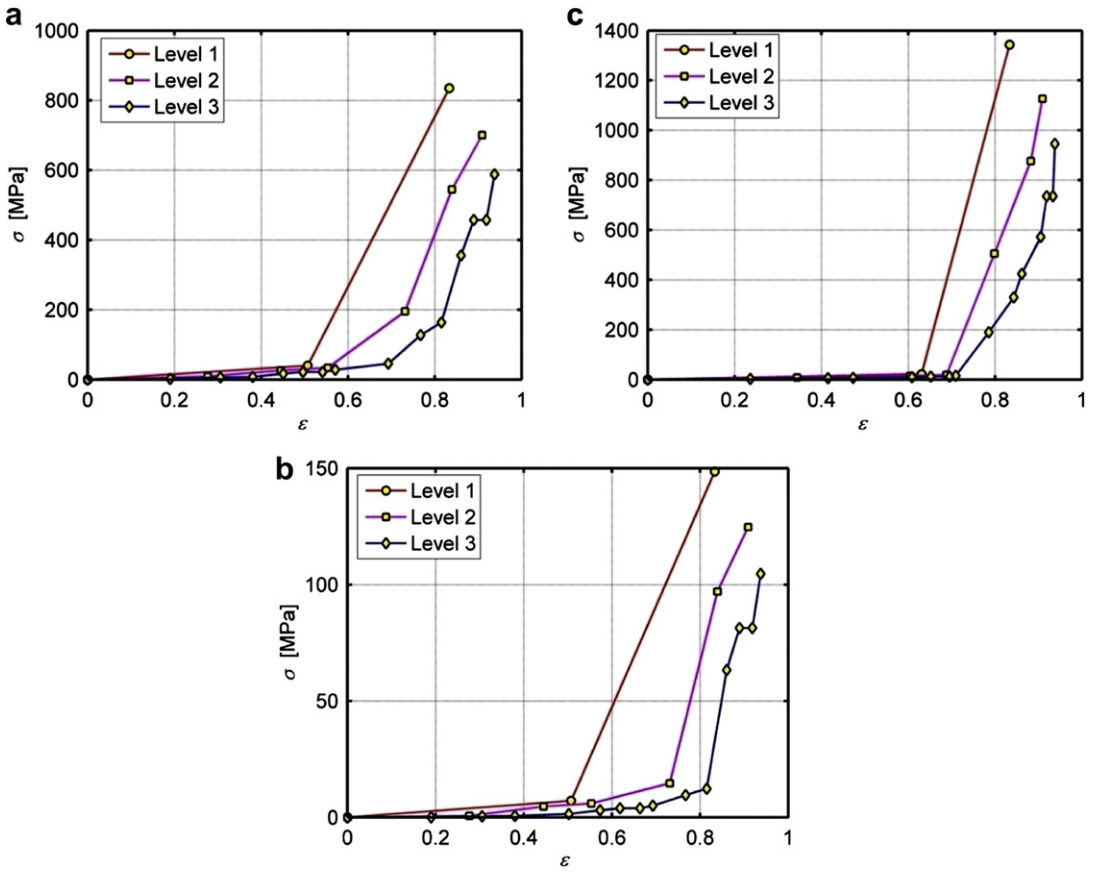

Fig. 10. Stress/strain curve *vs* level n: (a) $h/l = 1.0$, $t/l = 0.4$, $\theta = 40^\circ$; (b) $h/l = 1.0$, $t/l = 0.3$, $\theta = 40^\circ$; (c) $h/l = 2.0$, $t/l = 0.4$, $\theta = 40^\circ$.

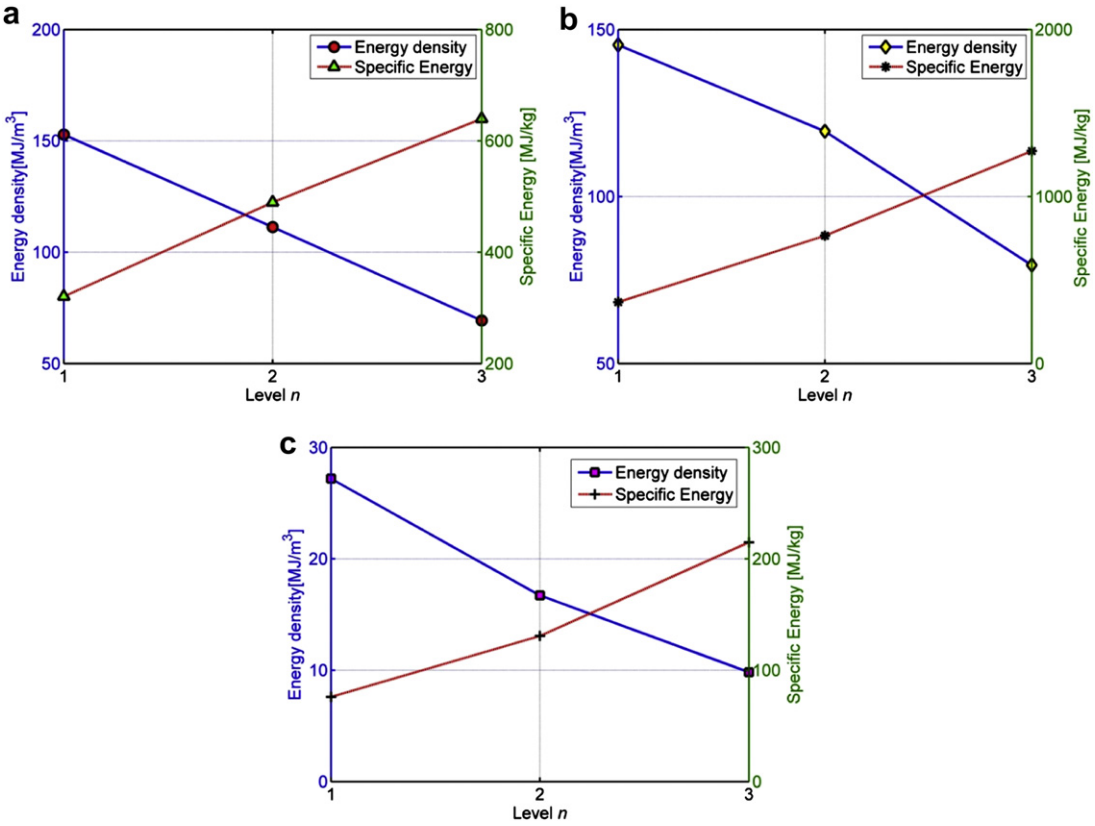

Fig. 11. Energy density and specific energy *vs* level n: (a) $h/l = 1.0$, $t/l = 0.4$, $\theta = 40^\circ$; (b) $h/l = 1.0$, $t/l = 0.3$, $\theta = 40^\circ$; (c) $h/l = 2.0$, $t/l = 0.4$, $\theta = 40^\circ$.

a higher strength-to-density ratio. This is because increasing h/l provides a lower density, and the influence on the density is stronger than that on the strength. We can also see that the influences on the strength-to-density ratio from the other geometrical parameters (θ or t/l) are similar to those reported in Fig. 6a,c, since the strength increment prevails on the density increment

3.3. Progressive buckling collapse

Compared with the first buckling stress, the progressive failure of the hierarchical honeycomb is more complex. Thus, due to this complexity, the calculation is here simplified by neglecting the influences produced by the collapsed columns (e.g., a length modification or a load redistribution in the surviving columns) and plotting the stress vector $(\overrightarrow{\sigma_{cr}^{(n)}}, \overrightarrow{\sigma_{cr}^{(n-1)}}, \ldots, \overrightarrow{\sigma_{cr}^{(1)}}, \overrightarrow{\sigma_{cr}^{(0)}})$ in ascending order with corresponding normalized strain $(\sum \Delta\varepsilon = 1)$ obtained from the vector $(\overrightarrow{\Delta\varepsilon_{cr}^{(n)}}, \overrightarrow{\Delta\varepsilon_{cr}^{(n-1)}}, \ldots, \overrightarrow{\Delta\varepsilon_{cr}^{(1)}}, \overrightarrow{\Delta\varepsilon_{cr}^{(0)}})$. Note that this simplified assumption is conservative. Here, we investigate a three-level self-similar honeycomb and treat 14 (8 + 4 + 2) different columns, due to the symmetry, see Fig. 8.

Note that:

$$h^{(i)}/l^{(i)} = m_2^{(i)}/m_1^{(i)} = h/l \tag{32}$$

Considering $l^{(3)} = 30$ mm and $m_1^{(i)} = 3$ in the example, $h^{(i)}$, $l^{(i)}$ and $m_2^{(i)}$ could be obtained according to the self-similar condition (32). The parametric analysis of the progressive failure is reported in Fig. 9a–c, in which each point corresponds to a column (Fig. 8); in particular, the experimental stress/strain curve measured by Easterling et al. (1982) is compared with our prediction for $\overrightarrow{\chi} = (20^\circ, 1.0, 0.4)$ (Fig. 9d). In Fig. 9a–c, b_{ij} denote the collapsed columns in the hierarchical honeycomb, as described in Fig. 8. To some extent, Fig. 9 reflects the degree of graceful failure quantitatively.

3.4. Constitutive laws and deformation energy

In addition, employing the same procedure of Section 3.3, we have investigated the stress/strain curves (Fig. 10) and absorbed energy density (absorbed energy per unit volume) or specific energy (absorbed energy per unit mass) (Fig. 11) for different levels n, from one to three. We have found that increasing the hierarchical level n, the energy density decreases but the specific energy increases. This suggests that hierarchical cellular solids are expected to have superior properties as energy-absorption light materials. Note that a compromise between energy density and specific energy is reached for two hierarchical levels, as observed in wood and grass stem, Fig. 2.

4. Conclusions

In this paper, we derive the buckling stresses and strains of hierarchical honeycomb materials. Parametric analyses are discussed for a two-level or three-level hierarchical honeycomb material, respectively. The former is employed to investigate the geometrical influences on the local buckling stress and mechanical efficiency. In general, they are improved by increasing the parameters except that increasing h/l results in a lower local buckling stress and the transverse compression strength of natural wood agrees well with our results. The latter model is considered to investigate the geometrical influences on the progressive collapse. Finally, the study on the stress/strain law and deformation energy shows that increasing hierarchical level n induces lower energy density but higher specific energy. The results indicate that the mechanical behaviors of the hierarchical structure can be tuned at each hierarchical level and thus is attractive for designing a new class of light but effective energy-absorption materials.

It is worth to say that the model considers hierarchical more than fractal architectures, to be more general and closer to the real world. However, geometrical self-similarity would lead to fractals. Thus fractals could be treated in our general hierarchical model as limiting cases (see also Pugno, 2006). Also including a filling of matrix in the present structure could show the existence of an optimal toughness, as discussed by Zhang et al. (2011).

Acknowledgments

NMP is supported by the European Research Council grant BIHSNAM. The authors wish to thank Luca Boarino and Emanuele Enrico at NanoFacility Piemonte, INRiM, a laboratory supported by the Compagnia di San Paolo, for the SEM images in Fig. 1.

References

Ashby, M.F., 2010. Materials Selection in Mechanical Design, fourth ed. Butterworth-Heinemann, Burlington.
Budiansky, B., 1999. On the minimum weights of compression structures. Int. J. Solids Struct. 36, 3677–3708.
Cai, X., 2007. Wood modifications for valued-added applications using nanotechnology-based approaches. PhD. Thesis, Université Laval, Canada.
Chang, C.H., 2005. Buckling of inclined columns. Lect Notes Appl. Comput. Mech. 22, 93–111.
Chen, Q., Pugno, N., 2011. A parametrical analysis on the elastic anisotropy of woven hierarchical tissues. Adv. Biomater.. doi:10.1002/adem.20108013.
Chen, Q., Pugno, N., 2012. Mechanics of hierarchical 3-D nanofoams. EPL 97, 260002.
Côté, F., Russel, B.P., Deshpande, V.S., Fleck, N.A., 2009. The through-thickness compressive strength of a composite sandwich panel with a hierarchical square honeycomb sandwich core. J. Appl. Mech. 76, 061004.
Easterling, K.E., Harrysson, R., Gibson, L.J., Ashby, M.F., 1982. On the mechanics of Basla and other wood. Proc. R. Soc. Lond A 383, 31–41.
Fabritius, H., Sachs, C., Romano Triguero, P., Raabe, D., 2009. Influence of structural principles on the mechanics of a biological fiber-based composite material with hierarchical organization: the exoskeleton of the lobster *Homarus americanus*. Adv. Mater. 21, 391–400.
Foo, C.C., Chai, G.B., Seah, L.K., 2007. Mechanical properties of Nomex material and Nomex honeycomb structure. Compos. Struct. 80, 588–594.
Gao, H., 2006. Application of fracture mechanics concepts to hierarchical biomechanics of bone and bone-like materials. Int. J. Fracture 138, 101–137.
Gibson, L.J., Ashby, M.F., Schajer, G.S., Robertson, C.J., 1982. The mechanics of two-dimensional cellular materials. Proc. R. Soc. Lond. A 382, 25–42.
Gibson, L.J., Ashby, M.F., 1997. Cellular Solids: Structure and Properties, second ed. Cambridge University Press, Cambridge.
Gibson, L.J., 2005. Biomechanics of cellular solids. J. Biomech. 38, 377–399.
Green, D.W., Winandy, J.E., Kretschmann, D.E., 1999. Mechanical properties of wood. In: Wood Handbook: Wood as an Engineering Material. U.S. Dapartment of Agriculture Forest Service, Forest Products Laboratory, Madison, WI chap. 4.
Krauss, S., Monsonego-ornan, E., Zelzer, E., Fratzl, P., hahar, R., 2009. Mechanical function of a complex three-dimensional suture joining the bony elements in the shell of the red-eared slider turtle. Adv. Mater. 21, 407–412.
Launey, M.E., Ritchie, R.O., 2009. On the fracture toughness of advanced materials. Adv. Mater. 21, 2103–2110.
Munch, E., Launey, M.E., Alsem, D.H., Saiz, E., Tomsia, A.P., Ritchie, R.O., 2008. Tough, bio-inspired hybrid materials. Science 322, 1516–1520.
Papka, S.D., Kyriakides, S., 1994. In-plane compressive response and crushing of honeycomb. J. Mech. Phys. Solids 42, 1499–1532.
Papka, S.D., Kyriakides, S., 1998a. In-plane crushing of a polycarbonate honeycomb. Int. J. Solids Struct. 35, 239–267.
Papka, S.D., Kyriakides, S., 1998b. Experiments and full-scale numerical simulations of in-plane crushing of a honeycomb. Acta Mater. 46, 2765–2776.
Pugno, N.M., 2006. Mimicking nacre with super-nanotubes for producing optimized super-composites. Nanotechnology 17, 5480–5484.
Pugno, N., Bosia, F., Carpinteri, A., 2008. Multiscale stochastic simulations for tensile testing of nanotube-based macroscopic cables. Small 4, 1044–1052.
Pugno, N., Carpinteri, A., 2008. Design of micro-nanoscale bio-inspired hierarchical materials. Phil. Mag. Lett. 88, 397–405.
Raabe, D., Sachs, C., Romano, P., 2005. The curstacean exoskeleton as an example of a structurally and mechanically graded biological nanocomposite material. Acta Mater. 53, 4281–4292.
Ritchie, R.O., Buehler, M.J., Hansma, P., 2009. Plasticity and toughness in bone. Phys. Today 62, 41–47.

Sen, D., Garcia, A., Buehler, M.J., 2011. Mechanics of nano-honeycomb silica structures: a size-dependent brittle-to-ductile transition. J. Nanomech. Micromech. 1, 112–118.
Smith, B.L., Schaffer, T.E., Viani, M., Thompson, J.B., Frederick, N.A., Kindt, J., Belcher, A., Stucky, G.D., Morse, D.E., Hansma, P.K., 1999. Molecular mechanistic origin of the toughness of natural adhesives, fibres and composites. Nature 399, 761–763.
Taylor, C.M., Smith, C.W., Miller, W., Evans, K.E., 2011. The effects of hierarchy on the in-plane elastic properties of honeycombs. Int. J. Solids Struct. 48, 1330–1339.
Timoshenko, S.P., Gere, J.M., 1961. Theory of Elastic Stability. McGraw-Hill, New York.
Tolf, G., 1985. Saint-Venant bending of an orthotropic beam. Compos. Struct. 4, 1–14.
Warren, W.E., Kraynik, A.M., 1987. Foam mechanics: the linear elastic response of two-dimensional spatially periodic cellular materials. Mech. Mater. 6, 27–37.
Xue, Z.Y., Hutchinson, J.W., 2006. Crush dynamics of square honeycomb sandwich cores. Int. J. Numer. Methods Eng. 65, 2221–2245.
Yao, H., Dao, M., Carnelli, D., Tai, K., Ortiz, C., 2011. Size-dependent heterogeneity benefits the mechanical performance of bone. J. Mech. Phys. Solids 59, 64–74.
Zhang, J., Ashby, M.F., 1992. Buckling of honeycombs under in-place biaxial stresses. Int. J. Mech. Sci. 34, 492–509.
Zhang, Z., Zhang, Y., Gao, H., 2011. On optimal hierarchy of load-bearing biological materials. Proc. R. Soc. B 278, 519–525.